Gamow-Teller transitions from the ^{14}N ground state to the ^{14}C ground and excited states

Yoshiko Kanada-En'yo
Department of Physics, Kyoto University, Kyoto 606-8502, Japan

Tadahiro Suhara
Matsue College of Technology, Matsue 690-8518, Japan

(Received 20 January 2014; revised manuscript received 3 March 2014; published 10 April 2014)

Gamow-Teller transitions from the ^{14}N ground state to the ^{14}C ground and excited states were investigated, based on the model of antisymmetrized molecular dynamics. The calculated strengths for the allowed transitions to the 0^+, 1^+, and 2^+ states of ^{14}C were compared with the experimental data measured by high-resolution charge-exchange reactions. The calculated GT transition to the 2^+_1 state is strong while those to the $0^+_{2,3}$ and $2^+_{2,3}$ states having dominant $2\hbar\omega$ excited configurations are relatively weak. The present calculation cannot describe the anonymously long lifetime of ^{14}C, though the strength of the ^{14}C ground state is somewhat suppressed because of the cluster (many-body) correlation in the ground states of ^{14}C and ^{14}N.

DOI: 10.1103/PhysRevC.89.044313 PACS number(s): 21.10.Hw, 21.60.−n, 23.40.−s, 27.20.+n

I. INTRODUCTION

In light-mass nuclei, cluster structures often appear in ground and excited states. Spatially developed cluster structures are found in excited states of stable and unstable nuclei, while cluster components are also contained in the ground states. The cluster component usually contains many-body correlation, and in terms of the spherical shell model, it is expressed by mixing of higher shell configurations beyond the simple $0\hbar\omega$ configuration. We call the correlation in the ground state caused by the cluster component "ground-state cluster correlation."

One of the typical examples of the ground-state cluster correlation is the 3α cluster structure in ^{12}C; such cluster structures develop remarkably in excited states of ^{12}C. Also in the ground state, the 3α cluster component is significantly mixed into the $p_{3/2}$-shell closed configuration, which is the lowest state in the uncorrelated j-j coupling state. As a result of the mixing of the cluster component, the ground band of ^{12}C exhibits oblate deformation. This deformation can be easily understood by 3α cluster models, while it is difficult to describe such a deformation with many mean-field calculations such as the Hartree-Fock calculation, showing the spherical ground state of ^{12}C [1].

Also in ^{14}C, various cluster structures such as $^{10}\mathrm{Be}+\alpha$ and $3\alpha+2n$ have been suggested in excited states [2–6]. In our previous work [6], which employed a method of antisymmetrized molecular dynamics (AMD), we discussed not only the cluster structures in excited states but also the cluster component in low-lying states and showed that the ground and low-lying states contain the cluster component (the cluster correlation) even though ^{14}C is a neutron p-shell closed nucleus.

Recently, the Gamow-Teller (GT) transition strengths for excited states of light nuclei have been extensively studied by use of experiments on high-resolution charge-exchange reactions [7]. The observed B(GT) values can be useful information to clarify the structure of excited states. For $A=14$ nuclei, the GT strength distributions for excited states of ^{14}C and the mirror ^{14}O were studied in charge-exchange reactions on ^{14}N [8]. The measured B(GT) distributions to 0^+, 1^+, and 2^+ states up to the excitation energy $E_x=15$ MeV suggest the predominant strengths of 2^+ states. In comparison with the large-scale no-core shell-model (NCSM) calculation [9], it was shown that the NCSM calculation does not reproduce the detailed GT strengths of excited 0^+ and 2^+ states, and the possible need to include cluster structure in these light nuclei was suggested [8].

As known from the anomalous long lifetime of ^{14}C, the strong suppression of the GT transition to the ground ^{14}C is another issue to be solved. The GT strength for the ground-ground transition from ^{14}N to ^{14}C is several orders smaller than the simple shell-model calculation without fine-tuning of interaction [9–13]. It was suggested that the GT matrix element can vanish because of the accidental cancellation of the matrix element in the p-shell configurations [11]; the vanishing was demonstrated by tuning the spin-orbit and tensor forces and also shown recently by adjusting the three-body terms in chiral effective field theory in both the conventional shell model and large-scale shell model calculations [9,11–16].

In spite of sophisticated works with NCSM focusing on the GT strength for the ground-ground transition, the GT transitions to excited states of ^{14}C have not been well investigated. The large-scale NCSM calculation including $6\hbar\omega$ model space for excited states was performed by Aroua *et al.* [9], and it suggests that the inclusion of higher shell configuration has significant effects on the GT strength for excited states as well as the ground state of ^{14}C. However, the calculation neither reproduces the experimental spectra of excited 0^+ and 2^+ states in the $E_x=6$–10 MeV region nor describes the GT strength distributions.

In this paper, we study the GT transitions from the 1^+ ground state of ^{14}N to the ground and excited 0^+, 1^+, and 2^+ states of ^{14}C based on a method of AMD [17,18]. The AMD method has proven useful for describing cluster states as well as shell-model states, and it is suitable for investigating cluster structures in excited states as well as the ground-state cluster correlation. For the study of the

ground and excited states of ^{14}C, we perform the variation after total-angular-momentum (spin) and parity projections in the AMD framework (AMD+VAP) [19]. We obtain the 0^+_1, 1^+_1, and 2^+_1 states with dominant $0\hbar\omega$ components and significant mixing of higher shell components coming from the cluster components. We also obtain the $0^+_{2,3}$ and $2^+_{2,3}$ states with developed cluster structures containing dominant $2\hbar\omega$ components. The calculated energy spectra and GT strengths are compared with the experimental data and also with the large-scale NCSM calculation including $6\hbar\omega$ configurations. We also apply the generator coordinate method (GCM) [20] to the AMD model with the constraint (constraint AMD+GCM) of the deformation parameters β and γ as done in the previous work [6,21]. The contributions of the cluster correlation to the GT transitions to the 0^+_1 and 2^+_1 states are discussed.

In the present work, we use a phenomenological effective nuclear interaction consisting of central and spin-orbit forces. The adopted central interaction is the modified Volkov force [22] supplemented by the finite-range spin-orbit force, which successfully reproduces the energy spectra of ^{12}C in the AMD+VAP calculation [19,23]. With such a simple effective interaction used in the present work, it is difficult to describe the vanishing of the GT transition to the ^{14}C ground state. For the ground state, we show only that the GT strength can be somewhat reduced by the ground-state cluster correlation but do not discuss the origin of the vanishing (the several-order reduction) of the GT strength, which may be caused by the accidental cancellation of GT matrix elements.

This paper is organized as follows. In the subsequent section, the formulation and Hamiltonian of the present calculation are explained. The results are shown in Sec. III. In Sec. IV, structures of the ground and excited states are discussed while focusing on the cluster correlation. The effect of the cluster correlation on the GT strengths is also discussed on the basis of the β-γ constraint AMD calculation. Finally, a summary is given in Sec. V.

II. FORMULATION

To describe ^{14}C and ^{14}N, we apply the AMD+VAP method. We also apply the β-γ constraint AMD+GCM method and obtain results similar to those for AMD+VAP result.

The AMD+VAP method is the same one used for the study of ^{12}C in Refs. [19,23], and the β-γ constraint AMD+GCM is basically the same as the method used in the previous work for ^{14}C [6]. For the details of these frameworks, the readers are referred to Refs. [6,18,19,21,23].

A. AMD wave functions

In the AMD method, a basis wave function of an A-nucleon system is described by a Slater determinant of single-particle Gaussian wave packets,

$$\Phi_{\rm AMD}(\mathbf{Z}) = \frac{1}{\sqrt{A!}}\mathcal{A}\{\varphi_1,\varphi_2,\ldots,\varphi_A\}. \tag{1}$$

The ith single-particle wave function φ_i is written as a product of spatial, intrinsic spin, and isospin wave functions:

$$\varphi_i = \phi_{\mathbf{X}_i}\chi_i\tau_i, \tag{2}$$

$$\phi_{\mathbf{X}_i}(\mathbf{r}_j) = \left(\frac{2\nu}{\pi}\right)^{4/3}\exp\left\{-\nu\left(\mathbf{r}_j - \frac{\mathbf{X}_i}{\sqrt{\nu}}\right)^2\right\}, \tag{3}$$

$$\chi_i = \left(\frac{1}{2}+\xi_i\right)\chi_\uparrow + \left(\frac{1}{2}-\xi_i\right)\chi_\downarrow. \tag{4}$$

$\phi_{\mathbf{X}_i}$ and χ_i are the spatial and spin functions, and τ_i is the isospin function fixed either up (proton) or down (neutron). The width parameter ν is fixed at the same value $\nu = 0.19\,\mathrm{fm}^{-2}$ as that used in the study of ^{12}C [23]. Accordingly, an AMD wave function is expressed by a set of variational parameters $\mathbf{Z} \equiv \{\mathbf{X}_1,\mathbf{X}_2,\ldots,\mathbf{X}_A,\xi_1,\xi_2,\ldots,\xi_A\}$ which express Gaussian center positions and spin orientations of A nucleons.

B. AMD+VAP method

In the AMD+VAP method, the energy variation is performed after the spin and parity projections in the AMD model as done in previous work on ^{12}C [19,23]. For the lowest J^π state, the parameters $\mathbf{X}_i$ and $\xi_i (i = 1$–$A)$ are varied to minimize the energy expectation value of the Hamiltonian, $\langle\Phi|H|\Phi\rangle/\langle\Phi|\Phi\rangle$, with respect to the spin-parity eigenwave function projected from an AMD wave function; $\Phi = P^{J\pi}_{MK}\Phi_{\rm AMD}(\mathbf{Z})$. Here, $P^{J\pi}_{MK}$ is the spin-parity projection operator. After the energy variation by a frictional cooling method [18], the optimum AMD wave function $\Phi_{\rm AMD}(\mathbf{Z}^{J^\pi})$ is obtained. The obtained wave function $\Phi_{\rm AMD}(\mathbf{Z}^{J^\pi})$ approximately describes the intrinsic wave function for the lowest J^π state. For higher J^π_k $(k \geqslant 2)$ states, the energy variation after the spin and parity projections is performed for the component orthogonal to the lower J^π states. Then, for each J^π_k, the optimum parameter solution $\mathbf{Z}^{J^\pi_k}$ is obtained. In the case of ^{14}C, we perform the VAP calculations for the $0^+_{1,2,3}$, 1^+_1, and $2^+_{1,2,3}$ states and obtain seven sets of parameters $\mathbf{Z}$. After the VAP procedure, final wave functions are calculated by superposing the spin-parity eigenwave functions projected from these seven AMD wave functions $\Phi_{\rm AMD}(\mathbf{Z}^\alpha)$ obtained by the VAP. Here α is the label for seven VAP states, $\alpha = 0^+_{1,2,3}$, 1^+_1, and $2^+_{1,2,3}$ states. Namely, the final wave functions for the J^π_n states are expressed as

$$\left|\Psi^{^{14}\mathrm{C}}_{\rm VAP}\left(J^\pi_n\right)\right\rangle = \sum_{K,\alpha} c^{J^\pi}_n(K,\alpha)\left|P^{J\pi}_{MK}\Phi_{\rm AMD}(\mathbf{Z}^\alpha)\right\rangle, \tag{5}$$

where the coefficients $c^{J^\pi}_n(K,\alpha)$ are determined by diagonalization of norm and Hamiltonian matrices. For the ground state of ^{14}N, the VAP is performed for $J^\pi = 1^+$. Then, the ^{14}N ground-state wave function is described by the spin-parity eigenstate projected from the $\Phi_{\rm AMD}(\mathbf{Z}^{1^+})$ with K mixing.

C. β-γ constraint AMD+GCM

In the β-γ constraint AMD+GCM method, the energy variation is performed after the parity projection but before the spin projection under certain constraints. Namely, we perform

the energy variation for the parity projected wave function, $\Phi = P^{\pi}\Phi_{\rm AMD}(\mathbf{Z})$ with the constraint on the quadrupole deformation parameters β and γ. Here, P^{π} is the parity projection operator. The deformation parameters β and γ are defined as

$$\beta\cos\gamma \equiv \frac{\sqrt{5\pi}}{3}\frac{2\langle z^2\rangle - \langle x^2\rangle - \langle y^2\rangle}{R^2}, \tag{6}$$

$$\beta\sin\gamma \equiv \sqrt{\frac{5\pi}{3}}\frac{\langle x^2\rangle - \langle y^2\rangle}{R^2}, \tag{7}$$

$$R^2 \equiv \frac{5}{3}(\langle x^2\rangle + \langle y^2\rangle + \langle z^2\rangle). \tag{8}$$

For a given set of constraint parameters (β_i,γ_i), we impose the constraints: $\beta\cos\gamma = \beta_i\cos\gamma_i$, $\beta\sin\gamma = \beta_i\sin\gamma_i$, and

$$\frac{\langle xy\rangle}{R^2} = \frac{\langle yz\rangle}{R^2} = \frac{\langle zx\rangle}{R^2} = 0. \tag{9}$$

After the energy variation with the constraints, we obtain the optimized wave function $\Phi = P^{\pi}\Phi_{\rm AMD}(\mathbf{Z}^{(\beta_i,\gamma_i)})$ for the ith set of deformation parameters (β_i,γ_i). For the constraint parameters (β_i,γ_i), we take the triangular lattice points with mesh size 0.05 on the β-γ plane as done in Refs. [6,21]. We truncate the $(\beta\cos\gamma,\beta\sin\gamma)$ region as $\beta_i\sin\gamma_i \leqslant -(\beta_i\cos\gamma_i - 1)/2$ and $\beta_i\sin\gamma_i \leqslant -(\beta_i\cos\gamma_i - 0.75)/2$ and use a total of 121 and 72 mesh points for ^{14}C and ^{14}N, respectively, to save numerical cost. These truncations do not affect the results of low-lying states.

To obtain the wave functions for J^{π}_k states, we superpose the spin-parity projected AMD wave functions $P^{J\pi}_{MK}\Phi_{\rm AMD}(\mathbf{Z}^{(\beta_i,\gamma_i)})$ using GCM [20]. Then the final wave functions for the J^{π}_n states are described as

$$\left|\Psi^{^{14}\rm C}_{\beta\gamma-\rm MC}(J^{\pi}_n)\right\rangle = \sum_{i,K} c^{J^{\pi}}_n(K,\beta_i,\gamma_i)\left|P^{J\pi}_{MK}\Phi_{\rm AMD}(\mathbf{Z}^{(\beta_i,\gamma_i)})\right\rangle, \tag{10}$$

where the coefficients $c^{J^{\pi}}_n(K,\beta_i,\gamma_i)$ are determined by solving the Hill-Wheeler equation, i.e., the diagonalization of the norm and Hamiltonian matrices. The final wave function $\Psi^{^{14}\rm C}_{\beta\gamma-\rm MC}(J^{\pi}_n)$ is the multiconfiguration (MC) state, which is expressed by the linear combination of various configurations $P^{J\pi}_{MK}\Phi_{\rm AMD}(\mathbf{Z}^{(\beta_i,\gamma_i)})$ obtained by the β-γ constraint AMD.

D. Effective interactions

We use the same effective nuclear interaction as that used in the previous calculation of ^{12}C [23]. It is the MV1 force [22] for the central force supplemented by the two-body spin-orbit force given by the two-range Gaussian form with the range parameters being the same as those of the G3RS force [24]. The Coulomb force is approximated by using a seven-range Gaussian form. The spin-orbit strengths are taken to be $u_I = -u_{II} = 3000$ MeV. The Majorana, Bartlett, and Heisenberg parameters in the MV1 force are taken to be (A) $m = 0.62$ and $b = h = 0.125$ as well as the parameters (B) $m = 0.62$ and $b = h = 0$ used in Ref. [23]. We also present the results with different Majorana parameters, (C) $m = 0.58$ and $b = h = 0.125$ and (D) $m = 0.58$ and $b = h = 0$ to show that the interaction parameter dependence is minor.

In the present work, the MV1 force is adopted as the effective central interaction instead of the Volkov force [25] used in the previous work on ^{14}C [6]. In Ref. [6], the excitation energies calculated with the β-γ constraint AMD using the Volkov no. 2 force largely overestimate the experimental excitation energies of ^{14}C. This may come from the overbinding problem of the Volkov force for heavier mass nuclei. The MV1 force is the interaction modified from the Volkov force, and it consists of the finite-range two-body force and the zero-range three-body term. The force reasonably reproduces the energy spectra of p-shell and sd-shell nuclei.

III. RESULTS

With the AMD+VAP method we calculate the 1^+ ground state of ^{14}N. The magnetic moment and electric quadrupole moment calculated with AMD+VAP using the set A interaction are $\mu = +0.34$ (μ_N) and $Q = +0.92$ (e fm^2). The calculated value of the μ moment reasonably agrees with the experimental value, $\mu_{\rm exp} = +0.40376100(6)$ (μ_N), while that of the Q moment somewhat underestimates the experimental one, $Q_{\rm exp} = +1.93(8)$ (e fm^2). The ground-state wave function for ^{14}N is dominated by D-wave component. A possible reason for the underestimation of the Q moment is that tail parts of radial wave functions of the last proton and neutron might be insufficient in the present result. We also apply the AMD+VAP method to the $0^+_{1,2,3}$, 1^+_1, and $2^+_{1,2,3}$ states of ^{14}C and calculate the GT transition strengths from the ^{14}N ground state to ^{14}C states as well as the $B(E2;2^+_1 \to 0^+_1)$ and $B(M1;1^+_1 \to 0^+_1)$. The GT transition strength B(GT) is given as

$$B(\rm GT) = \left(\frac{g_A}{g_V}\right)^2 \frac{1}{2J_i+1}|\langle J_f||\sigma\tau_{\pm}||J_i\rangle|^2. \tag{11}$$

Here $g_A/g_V = 1.251$ is the ratio of the GT to Fermi coupling constant. In principle, the GT transition from the $J^{\pi} = 1^+$, $T = 0$ state is allowed for $J^{\pi} = 0^+$, 1^+, and 2^+, $T = 1$ states.

The results of B(GT) for the transitions from ^{14}N(1^+_1) to ^{14}C($0^+_{1,2,3}$, 1^+_1, and $2^+_{1,2,3}$), $B(E2)$, $B(M1)$, and the excitation energies of ^{14}C are shown in Table I, compared with the experimental data. The theoretical values obtained by the AMD+VAP calculation using four sets of interaction parameters are listed. Properties of the ground and excited states of ^{14}C are not strongly dependent on the interaction parameters within the present calculation. The calculated results obtained the β-γ constraint AMD+GCM using the set A interaction are also shown in the table. They are qualitatively consistent with those obtained with the AMD+VAP calculations. Quantitatively, the AMD+VAP calculation gives about 1 MeV lower energy for the ground states than the AMD+GCM one with the same interaction. For such excited states as ^{14}C(0^+_3) and ^{14}C(2^+_3), the AMD+GCM calculation gives 1–2 MeV lower energies than the AMD+VAP. From the standpoint of variational principle, the AMD+VAP is better for low-lying states while the AMD+GCM is better for highly excited states. In general, the AMD+VAP gives better solutions for low-lying states than the AMD+GCM because the basis AMD wave

TABLE I. Excitation energies E_x (MeV) of ^{14}C, B(GT) from ^{14}N(1^+_1) to ^{14}C, $B(E2;2^+_1 \to 0^+_1)$ (e^2fm^4) and $B(M1;1^+_1 \to 0^+_1)$ (μ_N^2) of ^{14}C. The theoretical values calculated with AMD+VAP using the interactions from sets A, B, C, and D are shown as well as those calculated with the β-γ constraint AMD+GCM using the set A interaction. The experimental data are taken from Refs. [8,26].

	AMD+VAP(A)		AMD+VAP(B)		AMD+VAP(C)		AMD+VAP(D)		β-γ-AMD +GCM(A)		exp.	
	E_x	B(GT)	E_x	B(GT)	E_x	B(GT)	E_x	B(GT)	E_x	B(GT)	E_x	B(GT)
^{14}C(0^+_1)	0	0.07	0	0.09	0	0.12	0	0.13	0	0.16	0	1.90×10^{-6}
^{14}C(0^+_2)	10.3	0.001	10.5	0.003	10.9	0.001	10.8	0.002	9.0	0.0002	6.589	0.056
^{14}C(0^+_3)	16.0	0.00002	16.8	0.00003	16.5	0.0001	17.7	0.0001	14.2	0.00005		
^{14}C(2^+_1)	7.9	2.4	7.5	2.5	10.1	2.1	9.6	2.4	7.2	2.3	7.012	0.45
^{14}C(2^+_2)	11.2	0.24	11.5	0.17	11.7	0.75	11.9	0.42	9.7	0.33	8.318	0.37
^{14}C(2^+_3)	14.9	0.03	15.3	0.03	15.2	0.002	16.4	0.003	12.2	0.10	10.425	0.098
^{14}C(2^+_4)									14.4	0.04		
^{14}C(1^+_1)	12.2	0.21	12.8	0.22	14.5	0.31	15.1	0.32	12.9	0.25	11.306	0.072
		$B(E2)$		$B(E2)$		$B(E2)$		$B(E2)$		$B(E2)$		$B(E2)$
^{14}C;$2^+_1 \to 0^+_1$		6.6		7.3		4.1		4.9		7.4		3.74
		$B(M1)$		$B(M1)$		$B(M1)$		$B(M1)$		$B(M1)$		$B(M1)$
^{14}C;$1^+_1 \to 0^+_1$		1.6		1.5		1.8		1.7		1.4		0.39(9)

functions are optimized for the spin-parity eigenstates in the AMD+VAP (energy variation after the projection) but, in the AMD+GCM, they are obtained by the energy variation without the spin projection. Instead, the GCM has an advantage of the superposition of many AMD wave functions, which is efficient in particular for highly excited states. Because of the difference in the variation and the superposition, the excitation energies of ^{14}C are somewhat different between AMD+VAP and AMD+GCM. However, other properties are similar to each other and it may indicate that the wave functions obtained by the AMD+VAP and AMD+GCM are similar. We discuss the AMD+VAP result mainly and also show the AMD+GCM one to demonstrate that the difference is minor except for excitation energies. The main purpose of showing the AMD+GCM result is to discuss the effect of cluster correlation on GT strengths because, in the AMD+GCM framework, it is easy to compare the transition strengths calculated with and without the cluster correlation.

The $B(E2;2^+_1 \to 0^+_1)$ of ^{14}C is reasonably reproduced by calculations using sets (C) and (D) of interaction parameters while it is slightly overestimated by those with sets (A) and (B). The $B(M1;1^+_1 \to 0^+_1)$ of ^{14}C is overestimated with four sets of interaction parameters. It indicates that the present wave functions may not be precise enough for quantitative description of the ground-state properties.

The calculated B(GT) for ^{14}C(0^+_1) is relatively small compared with those for $J^\pi = 1^+_1$ and 2^+_1 states. However, the present calculations fail to describe the vanishing of the GT strength known from the anomalously long lifetime of ^{14}C. For ^{14}C(2^+_1), the GT strength is B(GT) = 2–3 in the present calculation and is larger than the experimental value B(GT) = 0.45 measured by charge-exchange reactions. We obtain the 0^+_2 and 2^+_2 states with dominant $2\hbar\omega$ neutron excited configurations around $E_x = 10$ MeV. The features of these two states, such as the 0^+-2^+ level spacing and the GT transition, reasonably agree with those of the experimental 0^+_2 and 2^+_2 states; therefore, we assign them to the experimental ^{14}C(0^+,6.6 MeV) and ^{14}C(2^+,8.3 MeV). We also obtain the 0^+_3 and 2^+_3 states dominated by $2\hbar\omega$ neutron excited configurations around $E_x = 15$ MeV.

The calculated B(GT) distributions for ^{14}N(1^+_1) $\to$ ^{14}C(0^+,1^+,2^+) obtained with the AMD+VAP and β-γ constraint AMD+GCM using the set A interaction are compared with the experimental data and the large-scale $6\hbar\omega$ NCSM calculation with AV8' interaction [9] in Fig. 1. Qualitative features of the B(GT) distributions obtained in the present calculations are in reasonable agreement with the experimental B(GT) distributions except for B(GT) for ^{14}C(2^+_1). The calculated B(GT) for the 2^+_1 state is largest and is as much as that of the NCSM calculation. In the experimental B(GT) distribution for 2^+ states, relatively larger populations were observed compared with 0^+ and 1^+ states. However, the calculations overestimate the absolute value of the experimental B(GT) for the 2^+_1 state. This might indicate that the descriptions of the final state [^{14}C(2^+_1)] and/or the initial state [^{14}N(1^+_1)] is not sufficient in the present calculations.

Compared with the NCSM calculation, the present B(GT) for ^{14}C(0^+_1) is the same order as that of the large-scale $6\hbar\omega$ NCSM calculation using the effective interaction derived from the AV8' interaction. It should be noted that the vanishing of the GT matrix element for ^{14}C(0^+_1) has been discussed in several NCSM studies by fine tuning of the interactions [9,13–16]. For 0^+_2 and 2^+_2 states, the correspondence to the experimental B(GT) distributions seems better in the present result than in the NCSM calculation. In the NCSM calculation, the corresponding states might be missing or their excitation energies might be overestimated. In the present results, 0^+_2 and 2^+_2 states contain cluster correlations resulting in the mixing of higher shell components of proton and neutron excitations. Usually, shell-model calculations are not suitable for describing such cluster states.

IV. DISCUSSION

In the present result, even the ground states of ^{14}C and ^{14}N have significant mixing of proton and neutron excitations

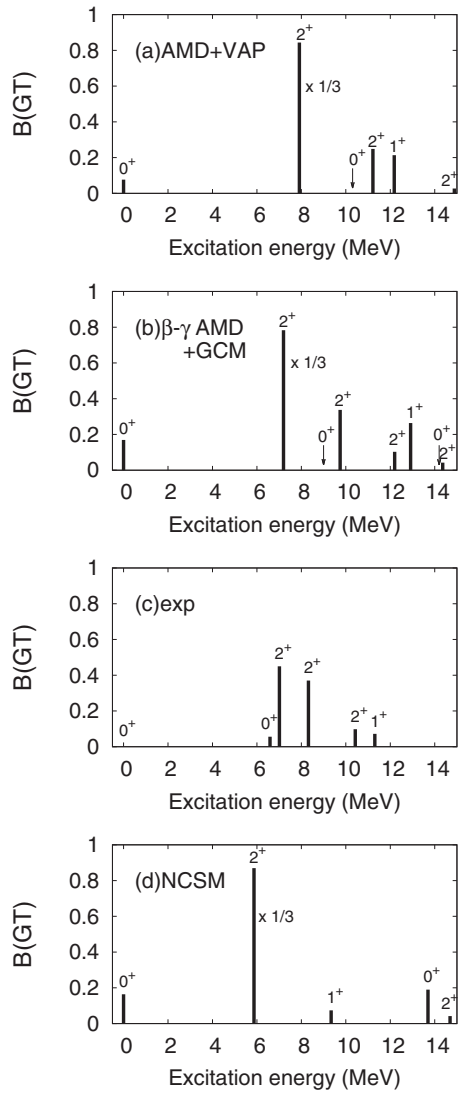

FIG. 1. The B(GT) distributions for transitions from the 1^+ ground state of ^{14}N to $J^\pi = 0^+,1^+$, and 2^+ states of ^{14}C. (a) The theoretical values calculated with the AMD+VAP using the set A interaction, (b) those calculated with the β-γ constraint AMD+GCM, (c) the experimental data taken from Refs. [8,26], and (d) the theoretical results from Ref. [9] of the NCSM calculation with the $6\hbar\omega$ model space using the effective interactions derived from Argonne V8' interaction.

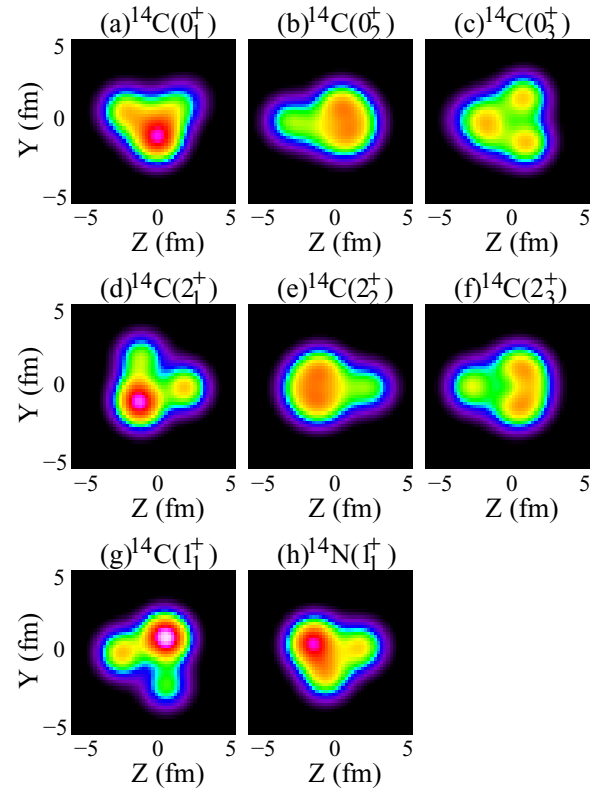

FIG. 2. (Color online) Density distribution for the intrinsic wave functions $\Phi_{\rm AMD}(\mathbf{Z}^{J^\pi_k})$ of ^{14}C and ^{14}N obtained with the AMD+VAP using the set A interaction. x, y, and z axes are chosen as $\langle x^2\rangle \leqslant \langle y^2\rangle \leqslant \langle z^2\rangle$ and the matter density integrated along the x axis is plotted on the z-y plane.

from the lowest $0\hbar\omega$ configuration because of the cluster correlations. In this section, we discuss intrinsic structures and cluster correlations in ^{14}C and ^{14}N. To show the mixing of excited configurations, we analyze the probability of higher shell components. The effect of the cluster correlations on the GT strengths for ^{14}C(0^+_1) and ^{14}C(2^+_1) is also discussed.

A. Intrinsic structure and cluster correlation

In the AMD+VAP calculation, the AMD wave function $\Phi_{\rm AMD}(\mathbf{Z}^\alpha)$ obtained by the VAP calculation for $\alpha = J^\pi_k$ is regarded as the intrinsic state of the J^π_k state. As seen in the density distributions of the intrinsic wave functions $\Phi_{\rm AMD}(\mathbf{Z}^\alpha)$ for ^{14}C and ^{14}N in Fig. 2, α-like or t-like cluster correlations are found even in the ground states of ^{14}C and ^{14}N. In the excited states of ^{14}C, further development of cluster structures is seen.

On the basis of the spherical harmonic oscillator (HO) shell model, those states contain significant components of excited configurations because of the cluster correlations. To discuss the higher-shell components beyond the lowest $0\hbar\omega$ configurations in each state, we calculate the occupation probability of HO quanta in the final wave function $\Psi^{^{14}{\rm C}}_{\rm VAP}(J^\pi_n)$ for the J^π_n state of ^{14}C. The calculations of the occupation probability are done following the method proposed by Suzuki *et al.* [27]. The occupation probability of a definite number of total HO quanta Q is given by the expectation value $\langle P_Q\rangle$ of the following projection operator P_Q to the eigenstate of the total HO quanta operator $\sum_i a^\dagger_i a_i$,

$$P_Q = \tfrac{1}{2\pi}\int_0^{2\pi} d\theta \exp\left[i\theta\left(\textstyle\sum_{i=1}^A a^\dagger_i a_i - Q\right)\right], \quad (12)$$

$$a^\dagger_i = \sqrt{m\omega/2\hbar}\,(x_i - ip_i/m\hbar), \quad (13)$$

$$a_i = \sqrt{m\omega/2\hbar}\,(x_i + ip_i/m\hbar), \quad (14)$$

where $\omega \equiv 2\hbar\nu/m$ (ν is the width parameter used in AMD wave functions). The occupation probability of total proton

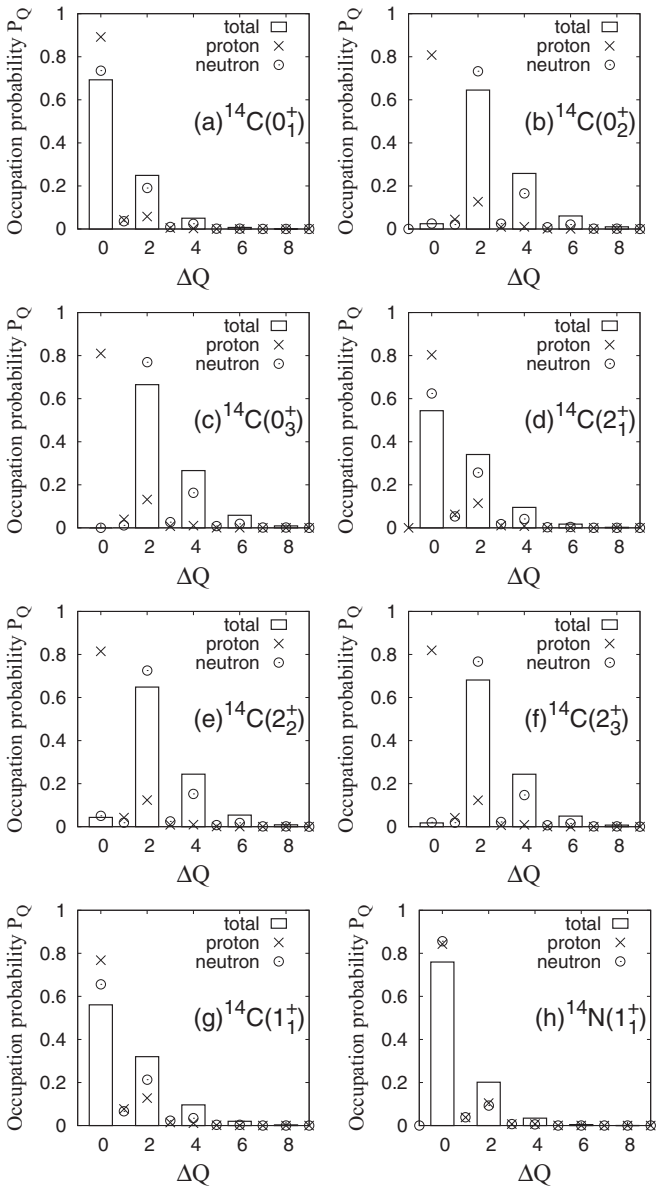

FIG. 3. Occupation probability $\langle P_Q \rangle$ for protons, neutrons, and total nucleons calculated with the AMD+VAP using the set A interaction. The calculated $\langle P_Q \rangle$ values are plotted as functions of $\Delta Q \equiv Q - Q_{\rm min}$ measured from the lowest allowed HO quanta $Q_{\rm min}$.

(neutron) HO quanta is calculated similarly by using the isospin projection operator.

We calculate $\langle P_Q \rangle$ for protons, neutrons, and total nucleons and plot the values as functions of $\Delta Q \equiv Q - Q_{\rm min}$ measured from the lowest allowed HO quanta $Q_{\rm min}$. $\langle P_Q \rangle$ for total nucleons stands for the component of ΔQ-$\hbar\omega$ configurations, and that for protons (neutrons) indicates the probability of proton (neutron) ΔQ-$\hbar\omega$ excitation. The results of the AMD+VAP states $\Psi^{^{14}{\rm C}}_{\rm VAP}(J^\pi_n)$ and $\Psi^{^{14}{\rm N}}_{\rm VAP}(1^+_1)$ obtained using the set A interaction are shown in Fig. 3.

It is found that the ground state ^{14}C(0^+_1) is not only dominated by the $0\hbar\omega$ component but also contains significant components, i.e., 25% and 5% of $2\hbar\omega$ and $4\hbar\omega$ excited configurations, respectively. In the higher shell components, the neutron excitation is dominant and the proton excitation is minor. The mixing of proton excitation is caused by the cluster correlation. Also the ground state of ^{14}N contains 20% of $2\hbar\omega$ excited configurations, a significant component.

In the excited states ^{14}C(2^+_1) and ^{14}C(1^+_1), the $0\hbar\omega$ component is dominant but is reduced to 50% because of the larger probability of excited configurations than the ground state. ^{14}C($0^+_{2,3}$) and ^{14}C($2^+_{2,3}$) have the dominant $2\hbar\omega$ configuration with the significant mixing of $4\hbar\omega$ and $6\hbar\omega$ configurations. In addition to the major neutron excitations, they also contain a 20% component of proton excitations because of the cluster correlation

Similar features for $\langle P_Q \rangle$ are found in the result of the β-γ constraint AMD+GCM calculation. Namely, significant higher shell components are contained even in the ground states of ^{14}C and ^{14}N. As described in Sec. II C, the final wave function $\Psi^{^{14}{\rm C}}_{\beta\gamma-{\rm MC}}(J^\pi_n)$ in the β-γ constraint AMD+GCM calculation is given by the superposition of various AMD configurations on the β-γ plane. In the framework of β-γ constraint AMD, the spherical $\beta = 0$ state corresponds to a $0\hbar\omega$ configuration state, while deformed states with finite β and/or γ values contain higher shell components in terms of the spherical HO shell model. For ^{14}C and ^{14}N systems, the finite β and/or finite γ states have cluster structure containing more components of higher shell configurations because of the cluster correlations. This means that in the β-γ constraint AMD+GCM, higher shell components beyond the $0\hbar\omega$ configuration are mixed in the ground-state wave function through the finite β and/or finite γ states in the superposition of basis AMD wave functions. Therefore, in this framework, the origin of the mixing of excited configurations can be understood by the deformation modes accompanied by cluster correlations.

In Fig. 4, we show the energy expectation values for the parity projected wave functions $P^\pi \Phi_{\rm AMD}(\mathbf{Z}^{(\beta_i,\gamma_i)})$ obtained by the β-γ constraint AMD, and those for the spin-parity projected wave functions $P^{J\pi}_{MK} \Phi_{\rm AMD}(\mathbf{Z}^{(\beta_i,\gamma_i)})$. As seen in the density distributions in Figs. 5 and 6, we obtain various structures having cluster correlations in the β-γ constraint AMD wave functions of ^{14}C and ^{14}N. In the energy surface before the spin projection [Figs. 4(a) and 4(d)], the spherical $\beta = 0$ state [Figs. 5(b) and 6(b)] is the energy minimum. On the other hand, in the $J^\pi = 0^+$ projected states of ^{14}C [Fig. 4(b)] and the $J^\pi = 1^+$ projected states of ^{14}N [Fig. 4(e)], the energy minima shift to the finite β and γ states at $(\beta_{\rm min}\cos\gamma_{\rm min}, \beta_{\rm min}\sin\gamma_{\rm min}) = (0.225, 0.130)$ for ^{14}C(0^+) and $(\beta_{\rm min}\cos\gamma_{\rm min}, \beta_{\rm min}\sin\gamma_{\rm min}) = (0.250, 0.087)$ for ^{14}N(1^+), which show α-like or t-like cluster correlations [Figs. 5(a) and 6(a)]. This indicates that the deformed states with the cluster correlations are favored in the calculation with the spin projection, though the spherical $0\hbar\omega$ states are favored in the model space without the spin projection. Moreover, on the β-γ plane, the J^π-projected energy surface is very soft over a wide area that covers various β-γ states having further developed cluster structures. For example, in the case of the $J^\pi = 0^+$ energy surface of ^{14}C, the energy soft area within a few MeV energy difference from the energy minimum covers $(\beta\cos\gamma, \beta\sin\gamma) = (0.4, 0.0), (0.325, 0.130)$,

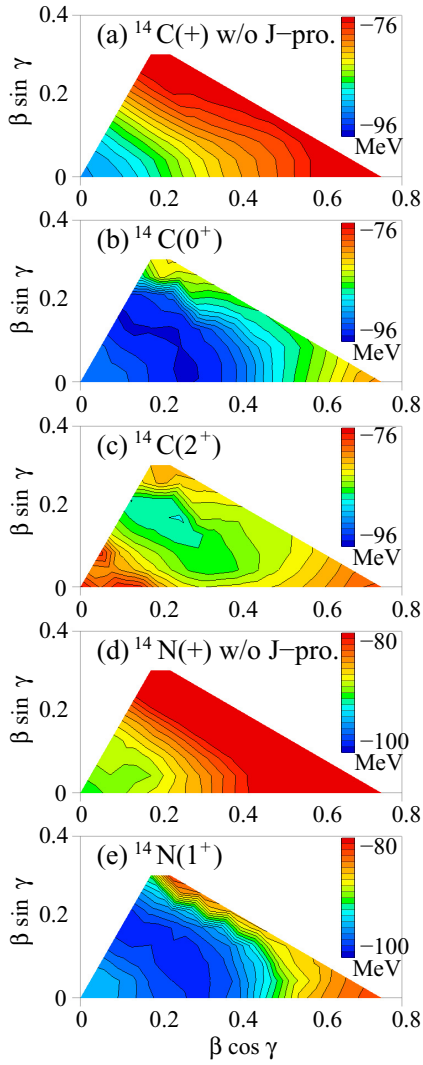

FIG. 4. (Color online) Energy expectation values calculated with the β-γ constraint AMD. (a) Energy for the positive-parity state projected from $\Phi_{\rm AMD}(\mathbf{Z}^{(\beta,\gamma)})$ of ^{14}C without the spin projection. (b) and (c) Energy for the 0^+ and 2^+ states of ^{14}C projected from $\Phi_{\rm AMD}(\mathbf{Z}^{(\beta,\gamma)})$. (d) Energy for the positive-parity state projected from $\Phi_{\rm AMD}(\mathbf{Z}^{(\beta,\gamma)})$ of ^{14}N without the spin projection. (e) Energy for the 1^+ state of ^{14}N projected from $\Phi_{\rm AMD}(\mathbf{Z}^{(\beta,\gamma)})$.

and (0.125,0.216) states [Figs. 5(c)–5(e)] as well as the $\beta = 0$ state. These states have α-like cluster structures and contribute to the significant mixing of the excited components such as the $2\hbar\omega$ and higher shell configurations in the final-state wave functions $\Psi^{^{14}\rm C}_{\beta\gamma-{\rm MC}}(J^\pi_n)$ as well as the initial-state wave function $\Psi^{^{14}\rm N}_{\beta\gamma-{\rm MC}}(J^\pi_n)$. It should be noted that although the ^{14}C wave functions with finite β and γ show α-like cluster structures, they do not have neutron and proton excitations of equal weight but do have dominant neutron and minor proton excitations. The reason is that neutrons in the α-like cluster are more largely affected by the antisymmetrization with neutrons inside the ^{10}Be core and, therefore, are more likely excited to higher configurations than protons.

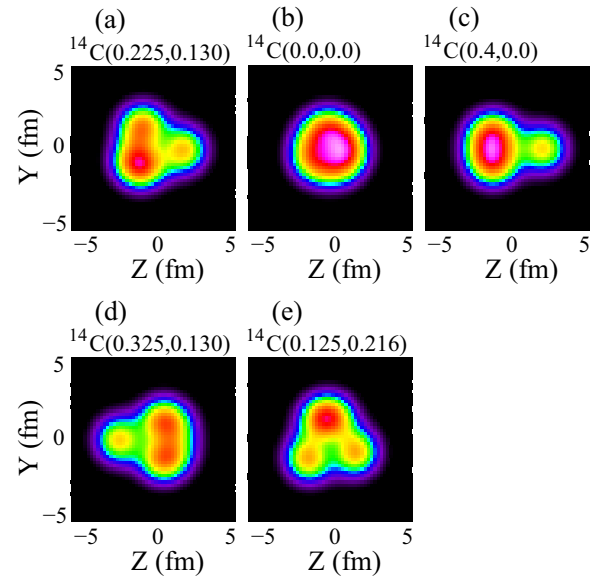

FIG. 5. (Color online) Density distribution for the intrinsic wave functions $\Phi_{\rm AMD}(\mathbf{Z}^{(\beta,\gamma)})$ of ^{14}C obtained with the β-γ constraint AMD using the set A interaction. The densities for the $J^\pi = 0^+$ energy minimum $(\beta_{\rm min}\cos\gamma_{\rm min}, \beta_{\rm min}\sin\gamma_{\rm min}) = (0.225,0.130)$ state and the spherical $\beta = 0$, prolate $(\beta\cos\gamma, \beta\sin\gamma) = (0.4,0.0)$, triaxial (0.325,0.130), and oblate (0.125,0.216) states are shown. x, y, and z axes are chosen as $\langle x^2\rangle \leqslant \langle y^2\rangle \leqslant \langle z^2\rangle$ and the matter density integrated along the x axis is plotted on the z-y plane.

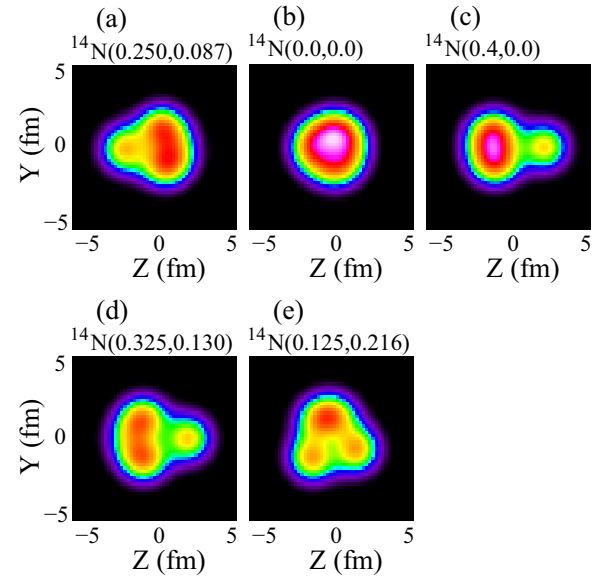

FIG. 6. (Color online) Density distribution for the intrinsic wave functions $\Phi_{\rm AMD}(\mathbf{Z}^{(\beta,\gamma)})$ of ^{14}N obtained with the β-γ constraint AMD using the set A interaction. The densities for the $J^\pi = 1^+$ energy minimum $(\beta_{\rm min}\cos\gamma_{\rm min}, \beta_{\rm min}\sin\gamma_{\rm min}) = (0.250,0.087)$ state, and the spherical $\beta = 0$, prolate $(\beta\cos\gamma, \beta\sin\gamma) = (0.4,0.0)$, triaxial (0.325,0.130), and oblate (0.125,0.216) states are shown. x, y, and z axes are chosen as $\langle x^2\rangle \leqslant \langle y^2\rangle \leqslant \langle z^2\rangle$, and the matter density integrated along the x axis is plotted on the z-y plane.

As shown in the occupation probability of total HO quanta (Fig. 3), higher shell components than $6\hbar\omega$ are very small even in the excited states, $^{14}C(0^+_{2,3})$ and $^{14}C(2^+_{2,3})$. It means that the cluster correlation in these states can be described within the $6\hbar\omega$ model space. On the other hand, the large-scale $6\hbar\omega$ NCSM calculation the NCSM predicts the $^{14}C(0^+_2)$ and $^{14}C(2^+_2)$ states at much higher excitation energies [9]. The inconsistency in the energy spectra might come from the difference in effective interactions. In the NCSM calculation, the effective interaction in the $6\hbar\omega$ model space is derived from the AV8' force by taking into account the effect of the higher shell truncation. Although the NCSM calculation is based on the realistic nuclear force and it reproduces low-lying spectra, it has not been confirmed yet that the derived effective interaction can quantitatively describe excitation energies of many-particle–many-hole states having cluster correlations. In the present calculation, we use the phenomenological effective interaction with which excitation energies of cluster states in such nuclei as ^{12}C, ^{16}O, ^{20}Ne, and ^{10}Be are reproduced well. More sophisticated study of the cluster correlation based on a realistic force should be done to understand the inconsistency.

B. Effect of cluster correlation on GT strength

As discussed above, the ground-state wave functions of ^{14}C and ^{14}N have cluster correlations that result in significant $2\hbar\omega$ and $4\hbar\omega$ components in terms of spherical HO shell-model expansion. In this section, we discuss the effect of the cluster correlations on the GT strengths for $^{14}C(0^+_1)$ and $^{14}C(2^+_1)$.

In the NCSM calculation in Ref. [9], the GT matrix elements are sensitive to the model space of shell-model configurations. For example, the $B(\mathrm{GT})$ for the GT transition to $^{14}C(0^+_1)$ is $B(\mathrm{GT}) = 2.518$ in the $0\hbar\omega$ model space NCSM calculations using two-body effective interactions derived from the AV8' force but it is reduced to $B(\mathrm{GT}) = 0.164$ in the $6\hbar\omega$ model space calculation. The $B(\mathrm{GT})$ values of the $6\hbar\omega$ NCSM calculation for $^{14}C(0^+_1)$ and $^{14}C(2^+_1)$ are eventually comparable with the present β-γ constraint AMD+GCM results in spite of differences in the effective interactions and the model space. Herein, we discuss the mixing effect of higher shell components on $B(\mathrm{GT})$ from the standpoint of cluster correlations.

In the β-γ constraint AMD and the AMD+VAP calculations, it is found that the deformed states with the cluster correlations are favored in the calculation with the spin projection though the spherical $0\hbar\omega$ states are favored in the model space without the spin projection. To see the effect of the cluster correlations in finite β and γ states on $B(\mathrm{GT})$, we show in Fig. 7 the $B(\mathrm{GT})$ values evaluated by the GT matrix element obtained using the single β-γ constraint AMD wave function for ^{14}N and that for ^{14}C, that is, the GT matrix element for the initial 1^+ state of ^{14}N projected from the β-γ constraint AMD wave function at the 1^+-projected energy minimum $(\beta_{\min}\cos\gamma_{\min}, \beta_{\min}\sin\gamma_{\min}) = (0.250, 0.087)$ and the final $J^\pi = 0^+$ and 2^+ states of ^{14}C projected from the β-γ constraint AMD wave function $\Phi_{\mathrm{AMD}}(\mathbf{Z}^{(\beta,\gamma)})$. We also show the $B(\mathrm{GT})$ given by the GT matrix element for the case in which the initial ^{14}N state is the spherical $\beta = 0$ state. Here the K mixing is taken into account.

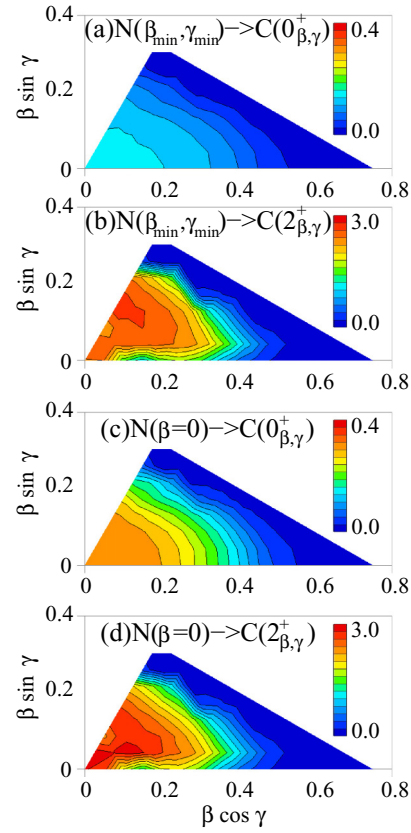

FIG. 7. (Color online) $B(\mathrm{GT})$ values evaluated by the GT matrix element obtained using the single β-γ constraint AMD wave function $\Phi_{\mathrm{AMD}}(\mathbf{Z}^{(\beta,\gamma)})$ for ^{14}N and that for ^{14}C. (a) and (b) $B(\mathrm{GT})$ values for the $J^\pi = 0^+$ and 2^+ states of ^{14}C projected from $\Phi_{\mathrm{AMD}}(\mathbf{Z}^{(\beta,\gamma)})$. The initial state is the 1^+ energy minimum state of ^{14}N at $(\beta_{\min}\cos\gamma_{\min}, \beta_{\min}\sin\gamma_{\min}) = (0.250, 0.087)$. Panels (c) and (d) are the same as panels (a) and (b) but the initial ^{14}N state is the 1^+ state projected from the spherical $\beta = 0$ wave function.

In both cases of initial ^{14}N states, the $\beta_{\min}$-$\gamma_{\min}$ and $\beta = 0$ states, the $B(\mathrm{GT})$ for $^{14}C(0^+)$ decreases as the deformation β of ^{14}C increases. Comparing the $B(\mathrm{GT})$ value for the final ^{14}C state at the spherical limit $\beta = 0$ with that for the ^{14}C state at the $J^\pi = 0^+$ energy minimum $(\beta_{\min}\cos\gamma_{\min}, \beta_{\min}\sin\gamma_{\min}) = (0.225, 0.130)$, the $B(\mathrm{GT})$ to $^{14}C(0^+)$ is reduced by 30% because of the cluster correlation in the final ^{14}C state. Note that the cluster correlation also changes components within $0\hbar$ configurations. Namely, in the case of $^{14}C(0^+)$, the $(p_{3/2})^4$ proton configuration (the j-j coupling state) is favored without cluster correlation, while the SU(3) limit p-shell configuration, the so-called L-S coupling p-shell state, is favored with the cluster correlation. The latter is the $(L = 0, S = 0)$ state in terms of the total orbital-angular momentum(L) and the total intrinsic spin (S). Since the GT transition from the dominant D-wave component of ^{14}N to the L-S coupling component (S-wave component) in $^{14}C(0^+)$ is forbidden, the GT transition is suppressed by the cluster correlation because of mixing of the L-S coupling component in the p shell as well as the mixing of the higher shell components. In the comparison of the $B(\mathrm{GT})$ for the initial ^{14}N state with $\beta = 0$ and $\beta_{\min}$-$\gamma_{\min}$, a 50%

reduction of B(GT) occurs because of the cluster correlation in the initial ^{14}N state.

In contrast to the B(GT) for ^{14}C(0^+), almost no reduction caused by cluster correlation is seen in the B(GT) for ^{14}C(2^+). In case of 2^+ state, possible four proton configurations in the p shell are $(L = 2, S = 0)$ and $(L = 1, S = 1)$ states. The former configuration is favored with the cluster correlation and it enhances the GT strength. Therefore, the cluster correlation enhances the $(L = 2, S = 0)$ component, resulting in the increase of the GT strength in $0\hbar\omega$ configurations, which compensates for the decrease of the GT strength due to the mixing of the higher shell component.

As mentioned before, the present results overestimate the experimental B(GT) for ^{14}C(0^+_1) and ^{14}C(2^+_1). Although the B(GT) for ^{14}C(0^+_1) can be somewhat reduced by the cluster correlation, the possible reduction is only a factor of 2−3 at most, and it is difficult to describe the anomalous suppression of the GT matrix element known from the long lifetime of ^{14}C. For the transition to ^{14}C(2^+_1), the B(GT) seems insensitive to the cluster correlation, and it is also difficult to quantitatively reproduce the experimental data in the present calculation.

V. SUMMARY

GT transitions from the ^{14}N ground state to the ^{14}C ground and excited states were investigated on the basis of the model of AMD. The AMD+VAP method and the β-γ constraint AMD+GCM were applied to 0^+, 1^+, and 2^+ states of ^{14}C as well as the ground state of ^{14}N. Both calculations show similar results.

The calculated strengths for the allowed transitions to 0^+, 1^+, and 2^+ states of ^{14}C were compared with experimental data measured by high-resolution charge-exchange reactions. The calculated GT transition to the 2^+_1 state is strong, whereas those to the $0^+_{2,3}$ and $2^+_{2,3}$ states having dominant $2\hbar\omega$ excited configurations are relatively weak. The B(GT) distributions to excited states of ^{14}C in the present calculations are in reasonable agreement with the experimental B(GT) distributions except for B(GT) for ^{14}C(2^+_1). The present calculation cannot describe the anonymously long lifetime of ^{14}C, though the GT strength of the ^{14}C ground state is relatively small compared with the $2^+_{1,2}$ and 1^+_1 states.

Compared with the large-scale NCSM calculations [9], the B(GT) values for ^{14}C(0^+_1) and ^{14}C(2^+_1) in the present calculation are almost the same as those in the $6\hbar\omega$ NCSM calculations. For higher 0^+ and 2^+ states, the present calculation shows a better description of the experimental B(GT) distributions in the $E_x \sim$ 10–15 MeV region.

It was found that the ground-state wave functions of ^{14}C and ^{14}N have cluster correlations that result in significant $2\hbar\omega$ and $4\hbar\omega$ components in terms of spherical HO shell-model expansion. In the excited states of ^{14}C, further development of cluster structures is seen.

The effect of the cluster correlations on the GT strengths for ^{14}C(0^+_1) and ^{14}C(2^+_1) was discussed. Although the B(GT) for ^{14}C(0^+_1) can be somewhat reduced by the cluster correlation, the possible reduction is only a factor of 2−3 at most, and it is difficult to describe the anomalous suppression of the GT matrix element known from the long lifetime of ^{14}C.

In the present calculation, we adopted the effective interactions composed of the central and spin-orbit forces but no tensor force. Since the tensor force may affect ground-state properties, in particular, spin properties, careful examination of its effect on GT strengths is a remaining problem. In the ^{14}N ground state, p-n correlation should be sensitive to the tensor force. If the spacial development of a dueteron-like cluster is enhanced by the tensor force, the GT transitions to ^{14}C(0^+_1) and ^{14}C(2^+_1) may be suppressed because their spatial overlap becomes small. It may also improve the description of the experimental Q moment of ^{14}N, which is underestimated in the present calculation. For more quantitative description of ground-state properties and GT transition strengths, explicit treatment of tensor force should be considered.

ACKNOWLEDGMENTS

The authors thank Prof. Fujita for valuable discussions. The computational calculations in this study were performed on the supercomputers at YITP, Kyoto University. This work was supported by a Grant-in-Aid for Scientific Research from the Japan Society for the Promotion of Science (JSPS). It was also supported by a Grant-in-Aid for the Global COE Program, "The Next Generation of Physics, Spun from Universality and Emergence," from the Ministry of Education, Culture, Sports, Science, and Technology (MEXT) of Japan.

[1] H. Sagawa, X. R. Zhou, X. Z. Zhang, and T. Suzuki, Phys. Rev. C **70**, 054316 (2004).
[2] N. Soic, M. Freer, L. Donadille, N. M. Clarke, P. J. Leask, W. N. Catford, K. L. Jones, D. Mahboub *et al.*, Phys. Rev. C **68**, 014321 (2003).
[3] D. L. Price, M. Freer, N. I. Ashwood, N. M. Clarke, N. Curtis, L. Giot, V. Lima, P. M. Ewan *et al.*, Phys. Rev. C **75**, 014305 (2007).
[4] W. von Oertzen, H. G. Bohlen, M. Milin, Tz Kokalova, S. Thummerer, A. Tumino, R. Kalpakchieva, T. N. Massey, Y. Eisermann, G. Graw, T. Faestermann, R. Hertenberger, and H.-F. Wirth, Eur. Phys. J. A **21**, 193 (2004).
[5] N. Itagaki, T. Otsuka, K. Ikeda, and S. Okabe, Phys. Rev. Lett. **92**, 142501 (2004).
[6] T. Suhara and Y. Kanada-En'yo, Phys. Rev. C **82**, 044301 (2010).
[7] Y. Fujita, T. Adachi, P. von Brentano, G. P. A. Berg, C. Fransen, D. De Frenne, H. Fujita, K. Fujita *et al.*, Phys. Rev. Lett. **95**, 212501 (2005).
[8] A. Negret, T. Adachi, B. R. Barrett, C. Baumer, A. M. van den Berg, G. P. A. Berg, P. von Brentano, D. Frekers *et al.*, Phys. Rev. Lett. **97**, 062502 (2006).
[9] S. Aroua, P. Navratil, L. Zamick, M. S. Fayache, B. R. Barrett, J. P. Vary, N. Smirnova, and K. Heyde, Nucl. Phys. A **720**, 71 (2003).

[10] D. R. Inglis, Rev. Mod. Phys. **25**, 390 (1953).
[11] B. Jancovici and I. Talmi, Phys. Rev. **95**, 289 (1954).
[12] W. M. Visscher and R. A. Ferrell, Phys. Rev. **107**, 781 (1957).
[13] M. S. Fayache, L. Zamick, and H. Muther, Phys. Rev. C **60**, 067305 (1999).
[14] J. W. Holt, G. E. Brown, T. T. S. Kuo, J. D. Holt, and R. Machleidt, Phys. Rev. Lett. **100**, 062501 (2008).
[15] J. W. Holt, N. Kaiser, and W. Weise, Phys. Rev. C **81**, 024002 (2010).
[16] P. Maris, J. P. Vary, P. Navratil, W. E. Ormand, H. Nam, and D. J. Dean, Phys. Rev. Lett. **106**, 202502 (2011).
[17] Y. Kanada-En'yo, H. Horiuchi, and A. Ono, Phys. Rev. C **52**, 628 (1995); Y. Kanada-En'yo and H. Horiuchi, *ibid.* **52**, 647 (1995).
[18] Y. Kanada-En'yo and H. Horiuchi, Prog. Theor. Phys. Suppl. **142**, 205 (2001); Y. Kanada-En'yo, M. Kimura and H. Horiuchi, C. R. Phys. **4**, 497 (2003); Y. Kanada-En'yo, M. Kimura, and A. Ono, Prog. Theor. Exp. Phys. **2012**, 01A202 (2012).
[19] Y. Kanada-En'yo, Phys. Rev. Lett. **81**, 5291 (1998).
[20] D. L. Hill and J. A. Wheeler, Phys. Rev. **89**, 1102 (1953); J. J. Griffin and J. A. Wheeler, *ibid.* **108**, 311 (1957).
[21] T. Suhara and Y. Kanada-En'yo, Prog. Theor. Phys. **123**, 303 (2010).
[22] T. Ando, K. Ikeda, and A. Tohsaki, Prog. Theory. Phys. **64**, 1608 (1980).
[23] Y. Kanada-En'yo, Prog. Theor. Phys. **117**, 655 (2007); **121**, 895(E) (2009).
[24] N. Yamaguchi, T. Kasahara, S. Nagata, and Y. Akaishi, Prog. Theor. Phys. **62**, 1018 (1979); R. Tamagaki, *ibid.* **39**, 91 (1968).
[25] A. B. Volkov, Nucl. Phys. **74**, 33 (1965).
[26] F. Ajzenberg-Selove, Nucl. Phys. A **523**, 1 (1991).
[27] Y. Suzuki, K. Arai, Y. Ogawa, and K. Varga, Phys. Rev. C **54**, 2073 (1996).